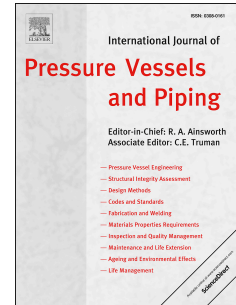# Journal Pre-proof

Residual stresses in austenitic thin-walled pipe girth welds: Manufacture and measurements

Foroogh Hosseinzadeh, Behrooz Tafazzoli-Moghaddam, Ho Kyeom Kim, Peter John Bouchard, Vasileios Akrivos, Anastasia N. Vasileiou, Mike Smith

This is a PDF file of an article that has undergone enhancements after acceptance, such as the addition of a cover page and metadata, and formatting for readability, but it is not yet the definitive version of record. This version will undergo additional copyediting, typesetting and review before it is published in its final form, but we are providing this version to give early visibility of the article. Please note that, during the production process, errors may be discovered which could affect the content, and all legal disclaimers that apply to the journal pertain.

Residual stresses in austenitic thin-walled pipe girth welds: Manufacture and measurements

Foroogh Hosseinzadeh[1*], Behrooz Tafazzoli-Moghaddam[1], Ho Kyeom Kim[1], Peter John Bouchard[1], Vasileios Akrivos[2], Anastasia N. Vasileiou[2], Mike Smith[2]

[1]The Open University, Walton Hall, Milton Keynes MK7 6AA UK, [2]University of Manchester, Sackville Street, Manchester, UK, M13 9PL.
[*]Corresponding author, email address: Foroogh.hosseinzadeh@open.ac.uk, contact number: +447588348005

Abstract

Determining residual stresses in thin-walled pipes is challenging. They are potentially difficult targets for simulation, because they may not behave as simple axisymmetric structures during welding. Thin-walled pipes are more sensitive to changes in the welding heat input than thick-walled pipes. They are also under-represented in the existing population of residual stress measurements used to generate upper bound residual stress profiles for structural integrity assessments. In this paper, residual stress characterisation of two thin-walled austenitic girth welded pipes is presented. The overall geometries of the two mock-up designs were the same; they differed in the linear heat input per pass and the total number of weld passes. The residual stress characterisation was carried out using two independent measurement techniques; the contour method and neutron diffraction. The multiple-cut contour strategy was implemented to measure the cross-sectional maps of hoop and axial stresses on axial-radial and hoop-radial planes respectively. The contour method results are compared with stresses measured using neutron diffraction and specific residual stress distribution signatures observed are discussed.

Keywords Contour Method, Neutron Diffraction, Weld Residual Stress, Structural Integrity, Finite Element Analysis.

1   Introduction

Welding is widely used in the fabrication of safety critical primary components in nuclear industry. Welding induced residual stresses play a key role in the life span of high integrity structures and can contribute to in-service degradation and premature failures. The R6 structural integrity assessment procedure [1] recognises the importance of weld residual stresses and requires an account of residual stresses in the safety critical weldments. The R6 recommended through-thickness residual stress profiles in the as-welded components is defined at various levels of sophistication and conservatism. The simplest approach, Level 1, assumes a uniformly distributed tensile stresses equal to the mean tensile strength value of the material. Level 2 residual stress profile is defined as an idealised upper bound profile to the data available from measurements and predictions of residual stresses for a set of as-welded joints. The R6 Level 3 residual stress profile is based on non-linear analytical modelling supported by experimental measurements.

The R6 Level 3 approach therefore reflects a more realistic hence less conservative distribution of residual stresses in welded components but depends on the availability of extensive computational modelling and detailed measurements. The treatment of residual stresses in assessment procedures

is often conservative and makes use of simple upper bound residual stress profiles with minimum effort due to the lack of available data.

Measured residual stress data from pipe girth weld mock-ups is surprisingly sparse [2], heavily skewed towards thick-walled pipes, and often obtained over 20 years ago when full-field residual stress measurements simply could not be made, and available techniques such as deep hole drilling and neutron diffraction were much less well-developed (see [3-5]). Only two thin-walled mock-ups (R/t>10) are available, of wall thicknesses >16mm, one of which is a double-vee preparation.

A broad range of reliable measured data are needed both for validation of R6 Level 3 (ie simulation) results, and to allow the development of less pessimistic upper bound R6 level two profiles (also found in BS7910 [6] and API 579 [7].

Although computational mechanics modelling has been increasingly used for weld residual stress predictions [8-10], uncertainties in finite element predictions remain a serious concern particularly for safety critical applications. The R6 structural integrity assessment procedure provides weld modelling guidelines for residual stress predictions for a range of welding processes. These guidelines impose strict validation requirements on such numerical predictions. The level of validation required depends on the structural integrity significance of weld residual stresses in the weldment being considered, but wholly unvalidated finite element predictions may not be used in structural integrity assessments of safety-critical components.

In the present paper, we focus on characterisation of residual stresses in thin-walled girth welded austenitic pipes for several reasons. First, prediction of residual stresses in thin-walled cylindrical weldments through Finite Element (FE) modelling is challenging. This is because they may not behave as simple 2-dimentional (2D) structures and hence an axisymmetric modelling simulation may not give a true representation of the state of residual stress and structural distortion. They require a 3D FE model with moving heat source for weld modelling for residual stress and distortion predictions [8, 9, 11, 12]. Second, despite thin-walled girth welded austenitic pipes are frequently used for pressurized fluid transportation in nuclear power plants the residual stress measurement data on these types of pipes is sparse to generate upper bound residual stress profiles for structural integrity assessment. Finally, post weld heat treatment of austenitic stainless-steel weldments is not feasible due to carbide re-precipitation preferentially in the grain boundaries at 550-750°C leading to chromium depletion adjacent to the grain boundaries rendering the alloy sensitisation to intergranular corrosion known as 'weld decay' [13]. Therefore, safety assessments must be carried out based on as-welded residual stress levels.

In this study, we designed and manufactured two mock-ups for the purpose of characterising as-welded residual stresses and to allow validation of finite element modelling of the welding process currently underway. The two pipes reported in this paper form part of a body of "modern" mock-ups manufactured and characterised as part of two European projects, STYLE and ATLAS+ [14, 15]. They were chosen to provide thin-walled equivalents (same materials, similar R, different t, to thick-walled pipes studied in those projects. The range of heat input (i.e the number of passes) was to assess sensitivity to this in a range that might be practicably welded.

Residual stress characterisation was carried out using two independent techniques with different characteristic errors: non-destructive neutron diffraction technique and strain-relief contour method.

The deep Hole Drilling (DHD) technique [16], commonly used to provide through thickness line profile of residual stress in thick and large nuclear components, is not feasible on the thin-walled mock-ups as the thickness of the pipes (9 mm) falls below the minimum required thickness for this technique.

The multi-cut contour method measurements, allowing full field mapping of individual stress components, are first-of-a kind in this type of pipe, and of considerable importance in assessing the significance of non-axi-symmetric behaviour in the residual stress field. This paper details the provenance of the welded mock-ups, their design and manufacture details (see Section 2), experimental residual stress measurement strategies together with the results of residual stress measurements presented in Section 3.

2   Manufacture of thin walled- welded pipes

2.1   Mock-ups, materials and preparation

Two similar metal pipe girth weld mock-ups were manufactured at The University of Manchester, to extend the range of geometries examined in the STYLE Framework 7 project [17]. The manufacturing of the mock-ups followed the procedures and the philosophy from previous projects [8, 11, 18, 19] to allow for subsequent modelling or characterisation work.

The mock-ups were made from AISI Type 316L austenitic stainless steel, using Gas Tungsten Arc Welding (GTAW); (i) one with 5 passes and low-heat input (5P-LH), and (ii) the other with 3 passes and high-heat input (3P-HH). The chemical composition and mechanical properties of the procured materials together with the original diameter and thickness dimensions of the mock-up pipes are provided in Table 1 and Table 2 respectively. The Young's modulus and Poisson ratio of the material were assumed as 204.5 GPa and 0.29 respectively as reported in [20].

The mock-ups were initially procured as 11 mm thick pipe and machined down to 9 mm prior to welding. The pipes were supplied in two batches with a relatively rough surface finish, and some variation in external diameter and thickness. The outer surface either side of the weld was skimmed to a smooth finish in a CNC lathe, while the inner bore was increased, again in a CNC lathe, to achieve the desired wall thickness over a longitudinal extent +/-30mm either side of the weld root. The pipes had been solution annealed at 1050°C as inferred from the mill certificates provided upon material procurement.

Table 1 Chemical composition of the AISI 316L pipes and the 316L filler wire (wt. %).

Specimens	C	Si	Mn	P	S	Cr	Ni	Mo	N
AISI 316L pipe	0.018	0.34	1.71	0.03	0.001	16.84	11.55	2.2	0.0523
SW-316L filler wire	0.015	0.45	1.8	0.025	0.02	18.5	11.5	2.6	-

Table 2 Mechanical properties at room temperature, and as-procured dimensions of the AISI 316L mock-up pipes and filler wire material.

Specimens	Outer Diameter (mm)	Wall thickness (mm)	0.2% stress (MPa)	1.0% stress (MPa)	UTS (MPa)	Elongation %
AISI 316L pipe	275	11.04	276	316	574	50.8
SW-316L filler wire			>420		~600	>30

The manufactured thin-walled pipes had an outer diameter of 275 mm, thickness 9 mm and length 350 mm and girth-welded at mid-length (see Figure 1). A conventional V-groove preparation was chosen, with a thickness of the land in the V-preparation of 1.5 mm (Figure 1b). The selection of the groove dimensions and the welding parameters was based on a number of trials performed both on plates and pipes. The main challenge was achieving good quality welds, with two significantly different sets of input parameters/heat inputs.

2.2 Welding process

The welding process was mechanised Gas Tungsten Arc Welding (GTAW) and was performed using a Polysoude robotic machine. The experiment was performed at The University of Manchester's Manufacturing Technology Research Laboratory (MTRL).

Two half-pipes were first tack welded together at 9 locations, circumferentially every 20° (Figure 1a). Two attachment plates were then tack-welded at one end of the pipe assembly (Figure 1), to allow clamping to the rotating manipulator. The welding torch remained stationary, in the 1G position, and the pipe was rotated beneath it. Two custom-made plexiglass covers were used to seal the pipe bore (Figure 1c), to retain shielding gas in the weld root region. Inert shielding gas was provided at both top (cap) and bottom (root) sides of the weld. The inert gas supply for the interior of the pipe was through a tube that was inserted through a hole in the cover, while that on the arc side was provided via the Polysoude welding head. The pipes were instrumented with thermocouples. A non-conventional set-up had to be employed, that allowed the data-logger and the wires to rotate without interfering with welding. The overall layout and the manufacturing drawing for the 9 mm thick pipes is shown in Figure 1.
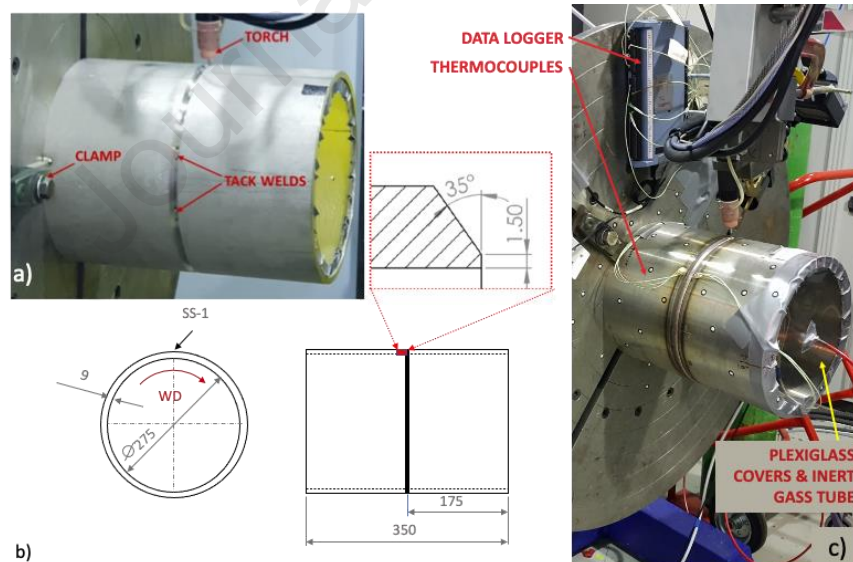

Figure 1 (a) General arrangement of mock-ups showing the clamping arrangements and tack weld, (SS-1: Pass-1 start position), (b)Drawing of the specimen and groove dimensions indicating the location of Pass-1 start position (SS1), (c) Welding set-up and instrumentation.

The welding parameters that were used are shown in Table 3 for both mock-ups. The Heat Input (kJ/mm) was calculated per pass, based on Equation 1. The same welding parameters, except the wire feed speed, were used for pass-1 in both cases, to ensure full-penetration. The subsequent passes

were performed with significantly different energy per pass. Although the welding parameters were pre-programmed, some degree of manual control was still exercised during welding, e. g. for setting the torch start position, ramping up/down, stopping each pass by overrunning 10-15 mm. A laser illumination system with a camera was installed and used, to closely monitor the melt pool quality. The weld groove geometry, the weld bead stacking pattern, quality and width of capping pass and photos of the welded mock-ups are shown in Figure 2.

$$ASME/AWS = \frac{Arc\ voltage * Arc\ current}{Travel\ speed}$$ Equation 1

Table 3 Basic welding parameters for manufacturing of the mock-ups.

| Parameter		Pass-1	Pass-2	Pass-3	Pass-4	Pass-5		Pass-1	Pass-2	Pass-3
Current (A)	5-pass low heat-input	250	200	200	200	200	3-pass high heat-input	250	220	200
High pulse time (ms)		300	300	300	300	300		300	300	300
Base current (A)		100	75	75	75	75		100	100	150
Base pulse time (ms)		300	300	300	300	300		300	300	300
Arc Voltage (V)		10	10.5	10.5	10.5	10.5		10	10.5	12
Wire feed speed (mm/min)		600	600	750	1200	1200		900	1200	3500
Base w.f.s. (mm/min)		362	362	362	362	362		362	362	1500
ASME/AWS Heat Input (kJ/mm)		**0.58**	**0.37**	**0.37**	**0.37**	**0.37**		**0.54**	**0.61**	**0.82**
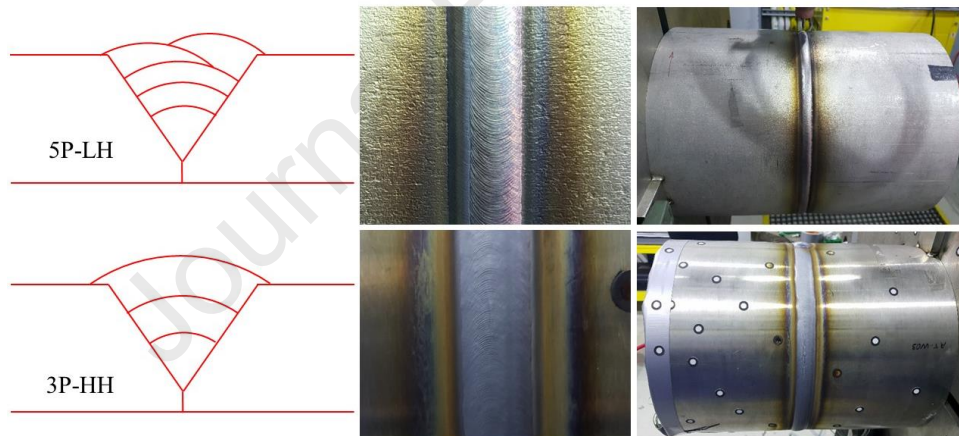
Figure 2 (Left) Stacking pattern, (Middle) quality and width of capping pass, (Right) photographs of the welded mock-ups for (Top) the 5-pass and the (Bottom) 3-pass cases.

An array of 16 thermocouples per pipe was used for recording the thermal transients. The deformation of the pipes was measured before welding, after each pass and after complete cool-down, using Creaform's Handyscan 700 hand-held laser scanner. Deformation data are shown on Table 4.

Table 4 Distortion and weld pass properties for the 3-pass high heat-input (3P HH) and the 5-pass low heat-input (5P LH) pipe girth welds.

Groove width (mm)	Axial Contraction (mm)	OD (mm) next to groove	Change in radius at WCL (mm)	Groove depth (mm)	Pass thickness (from groove depth)
3-pass high heat-input (3P HH)					

Before	11.19	0.00	274.76	0.00	7.96	0.0000
Pass-1	10.65	-0.54	273.95	-0.81	3.92	4.0361
Pass-2	9.81	-1.38	273.26	-1.50	1.95	1.9762
Pass-3	19.83 (weld cap)	n/a	272.98	-1.77	1.8553 (weld cap)	3.8040 (weld cap)
			5-pass low heat-input (5P LH)			
Before	10.99	0.00	274.85	0.00	5.93	0.0000
Pass-1	10.01	-0.99	273.78	-1.08	4.01	1.9210
Pass-2	9.46	-1.54	273.35	-1.50	2.60	1.4159
Pass-3	9.17	-1.83	273.48	-1.37	1.4560	1.1404
Pass-4	n/a	n/a	273.06	-1.80	0.0000	1.4560
Pass-5	13.25 (weld cap)	n/a	272.25	-2.60	1.6413 (weld cap)	1.6413 (weld cap)

3   Residual stress measurements

Residual stress measurements on both welded pipes were carried out using the contour method and neutron diffraction technique. The measurement strategy is illustrated in Figure 3. First each of the pipes was bisected using a single diametric contour cut to simultaneously map 2-Dimentional (2D) distribution of hoop residual stresses on two wall thicknesses. For both pipes the contour cut plane was located away from weld pass start/stop positions.

Neutron diffraction technique was conducted to measure three components of the stress tensor in the hoop, radial and axial directions. The neutron diffraction measurements were conducted at $90°$ away from the contour cut plane on the $180°$ shell containing weld pass 3 start/stop position for the 5P-LH pipe and on the $180°$ shell containing weld pass 1 and weld pass 2 start/stop position for the 3P-HH pipe. Finally, the contour method using multiple-cut approach was conducted to map axial stress distribution. Both 5P-LH $180°$ shells were cut at weld centreline whereas only the $180°$ shell containing weld pass 3 start/stop position for 3P-HH pipe was used for contour method axial stress measurement.

3P-HH pipe	5P-LH pipe
1) A single diametrical cut on the full pipe to measure hoop stress on two wall thicknesses 180˚ apart	1) A single diametrical cut on the full pipe to measure hoop stress on two wall thicknesses 180˚ apart
2) Extracting a slot from on the 180˚ shell containing weld pass 3 start/stop for neutron diffraction d_0 measurements	2) Extracting a slot from the 180˚ shell containing weld pass 2&5 start/stop for neutron diffraction d0 measurements
3) Neutron Diffraction measurement on the 180˚ shell containing weld pass 1&2 start/stop position at 90˚ from the cut plane	3) Neutron Diffraction measurement on the 180˚ shell containing weld pass 3 start/stop position at 90˚ from the cut plane
4) A circumferential contour cut on the 180˚ shell containing weld pass 3 start/stop position to measure axial stress	4) A circumferential contour cut on the 180˚ shell containing weld pass 3 start/stop position to measure axial stress
	5) A circumferential contour cut on the 180˚ shell containing weld pass 1,2,4, 5 start/stop position to measure axial stress

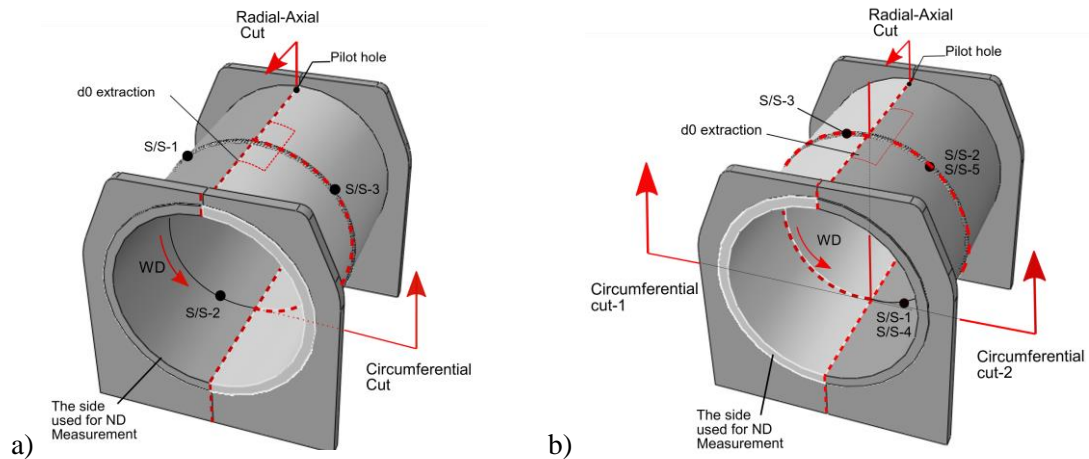3P-HH   5P-LH

Figure 3 (Top) Residual stress measurement strategy for the mock-ups, (Bottom) Schematic drawing of the welded mock-ups, (a) 3P-HH and (b) 5P-LH, showing the Welding Direction (WD), location of weld Start/Stop (S/S) positions and the contour cut planes and the 180° shells used for neutron diffraction measurement.

3.1 The contour method

The contour method, first presented in [21], is a destructive strain relief technique that allows characterising the cross-sectional distribution of residual stress along a plane of interest. The standard procedure for implementing the techniques involves: (i) sectioning the component into two halves along a plane of interest using electric discharge machining (EDM), (ii) measuring the resulting out-of-plane displacements of the created cut surfaces caused by the relaxation of residual stresses often using a Coordinate Measuring Machine (CMM) fitted with a touch probe or an optical sensor, (iii) processing the measured displacements to remove the effect of shear stress and artefacts introduced due to the wire EDM process or surface measurement; that is the data of the two cut surfaces are averaged, obvious noise and outliers removed and the data fitted to a smooth surface (e.g. bivariate splines, polynomials, Fourier series), (iv) applying the processed data as surface boundary conditions to a Finite Element (FE) model of one of the cut parts and conducting a fully elastic stress analysis to back calculate the original and pre-cut residual stress component acting normal to the plane of the cut [22].

An outstanding advantage of the contour method compared to other strain relief and diffraction-based techniques is that it can provide a cross-sectional map of residual stress using readily available equipment in most workshops. In theory the ability of the technique in measuring through thickness residual stresses is not limited by the size or geometrical complexity of components. Although only one component of the stress tensor, perpendicular to the cut surface, can be measured the technique has been expanded to measure multiple components of the stress tensor when combined with other techniques or using multiple cuts [23, 24]. In addition, unlike diffraction-based techniques, the contour method is not sensitive to microstructural variations that is often observed in weldments.

Like any other technique the accuracy and reliability of the contour method is based on several assumptions. Like other strain relief techniques, the contour method is prone to plasticity errors associated with inelastic redistribution of residual stress upon material removal [22, 25]. Another source of error specific to the contour method is associated with EDM induced cutting artefacts [25-27]. Extensive research work has been conducted on developing cutting strategies to mitigate or at

least minimise cutting induced plasticity errors [28-33]. Practical guidelines are also published providing measures to minimise or correct for cutting induced errors [22, 27].

3.1.1 Axial-radial cut plane for hoop stress measurement

In the present work the contour cutting and data analysis approach developed in [34] was conducted on the welded pipes to measure 2D map of hoop stress distribution over a radial-axial plane on two wall thicknesses 180° apart simultaneously. For each pipe, an embedded cutting strategy was conducted to provide self-constraint of the specimen during cutting, control the redistribution of residuals stresses and thereby reduce the risk of plasticity. Two diametrically opposite holes with 3 mm diameter at 10 mm from each end of the pipe were drilled. The embedded cutting strategy was made by starting the cut from one hole and cutting the pipe through to the other hole. Then the remaining ligaments at the ends of the pipe were sectioned, creating two 180° shells.

Sacrificial layers were bonded on the inner and outer surfaces of the pipe at the location of the cut plane to prevent cutting artefacts induced by wire entry and exit [26, 27]. All the contour cuts were carried out using an Agie Charmilles wire EDM machine (FI-440CS) with a 0.25 mm diameter brass wire. Custom made jigs were designed and manufactured to securely mount the pipes on the EDM bed and to prevent the parts moving during the EDM cutting [22, 34].

The out-of-plane displacement of both cut surfaces of each 180° shell cut part was measured in a common coordinate system to directly capture the contribution of distortion induced by the release of hoop bending moment as well as the self-equilibrated residual stresses. The contour results would therefore provide maps of hoop stress across the wall thickness on both sides of the pipe and automatically accounts for through-thickness hoop bending effects and its variation along the length of the pipe.

The out-of-plane displacements were measured using a Zeiss Eclipse CMM fitted with a Micro-Epsilon triangulating laser probe and a 2-mm diameter ruby-tipped Renishaw PH10M touch trigger probe. The touch trigger probe was used to measure the perimeter of the cut surfaces accurately at 0.25 mm pitch and the triangulating laser probe was used to measure the relaxation of the out-of-plane displacements on a 0.1 x 0.1 mm grid. The measured displacement data for each cut surface were then processed using the standard approach for contour measurement as described in section 3.1. Then, the processed displacement data from the three cut sequences were applied to 3D FE models of the cut parts as boundary conditions, but with reversed sign in the Z direction. Additional restraints in X and Y directions were applied to each model to stop rigid body motion (see Figure 4) and fully elastic stress analysis was conducted using ABAQUS 6.13 software [35].
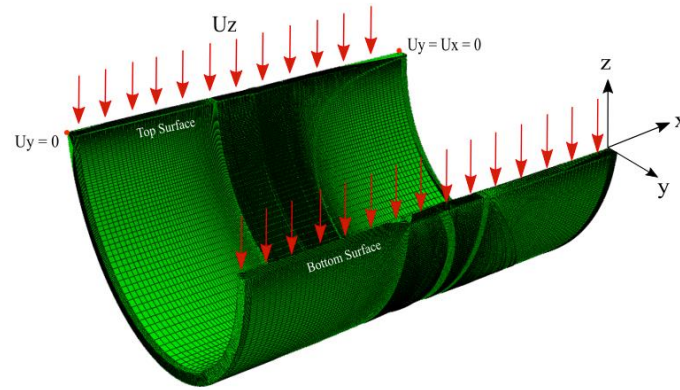
Figure 4 Finite Element 3D model and the mesh distribution for the hoop stress calculation. The model is fixed in X and Y directions at the points shown by red circles to avoid rigid body motion. The measured out-of-plane displacements are applied as surface boundary conditions to both the Top and Bottom surfaces in z direction.

Maps of hoop residual stress on the axial-radial plane using the single-cut approach for both the Top and Bottom cut surfaces for 3P-HH and 5P-LH mock-up pipes are shown in Figure 5. Note that the data in the vicinity of the pilot holes showed significant cutting induced artefacts. Hence, the stresses in these regions are discarded.
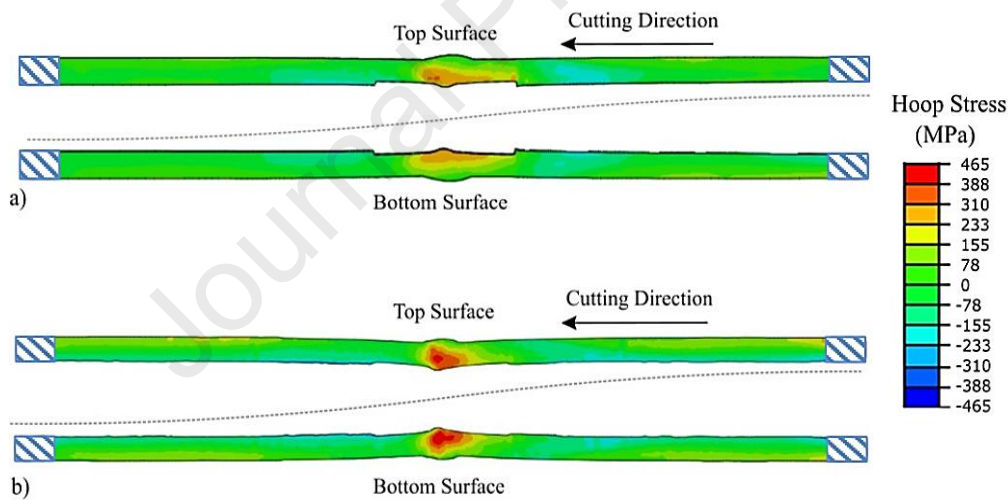
Figure 5 Map of hoop residual stress on a radial-axial plane showing the results on the Top and Bottom cut surfaces measured using the contour method for (a) 3P-HH and (b) 5P-LH mock-up pipes.

3.1.2 Radial-hoop cut plane for axial stress measurement

Following hoop stress measurement by the contour method (see section 3.1.1) and neutron diffraction measurements (see section 3.2) the two 180° shells of 5P-LH pipe and one 180° shell of 3P-HH pipe containing weld pass 3 start/stop position were further cut along the radial-hoop plane at weld centre line to map the axial stress distribution. Sacrificial materials were bonded on the outer and inner surfaces of the 180° shells at the location of the cut plane to create a uniform cross-section to prevent introducing wire EDM cutting artefacts (Figure 6).
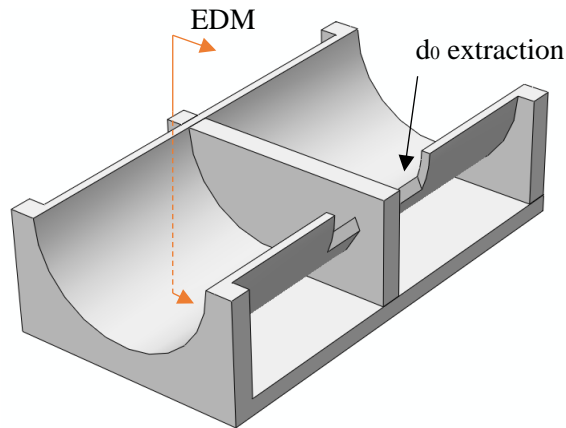
Figure 6 Schematic drawing of one of the 180° shell prepared for radial-hoop contour cut showing the bonded sacrificial material on the inner and outer surfaces and the bespoke jig used for secure clamping of the part on the EDM bed.

Likewise, the radial-hoop cuts were made using an Agie Charmilles wire EDM machine (FI-440CS) with a 0.25 mm diameter brass wire. All the cuts were conducted towards the side where a block of material was extracted for neutron diffraction d_0 measurements as indicated in Figure 6. The perimeter of the cut surfaces was measured at 0.25 mm pitch and the out-of-plane displacements of the cut surfaces were measured on a 0.1 x 0.1 mm grid.

For each cut part, a 3D model of 180° shell was created (from one end of the pipe to the cut surface at the weld centreline) by extruding the perimeter of the radial-hoop cut surface along the axial direction. To create the weld geometry, the radial-axial perimeter was used to cut-revolve the profile along 180° circumference of the pipe. The data processing and stress back-calculation steps followed the standard approach as described in Section 3.1.

The multiple-cut contour method approach was conducted for axial stress measurements. That is the relaxation of axial stresses due to the first contour cut was considered using the elastic superposition principle. Figure 7 shows the original distribution of axial stresses in the un-cut condition for the two mock-ups. The measured out-of-plane displacements at the start and end of the cut were impacted by wire cutting induced artefacts. Hence the back calculated stresses in these regions must be discarded and are not presented in Figure 7.
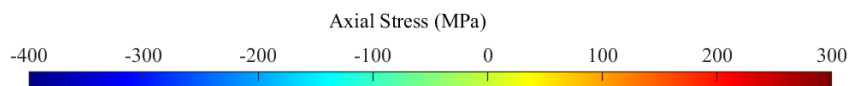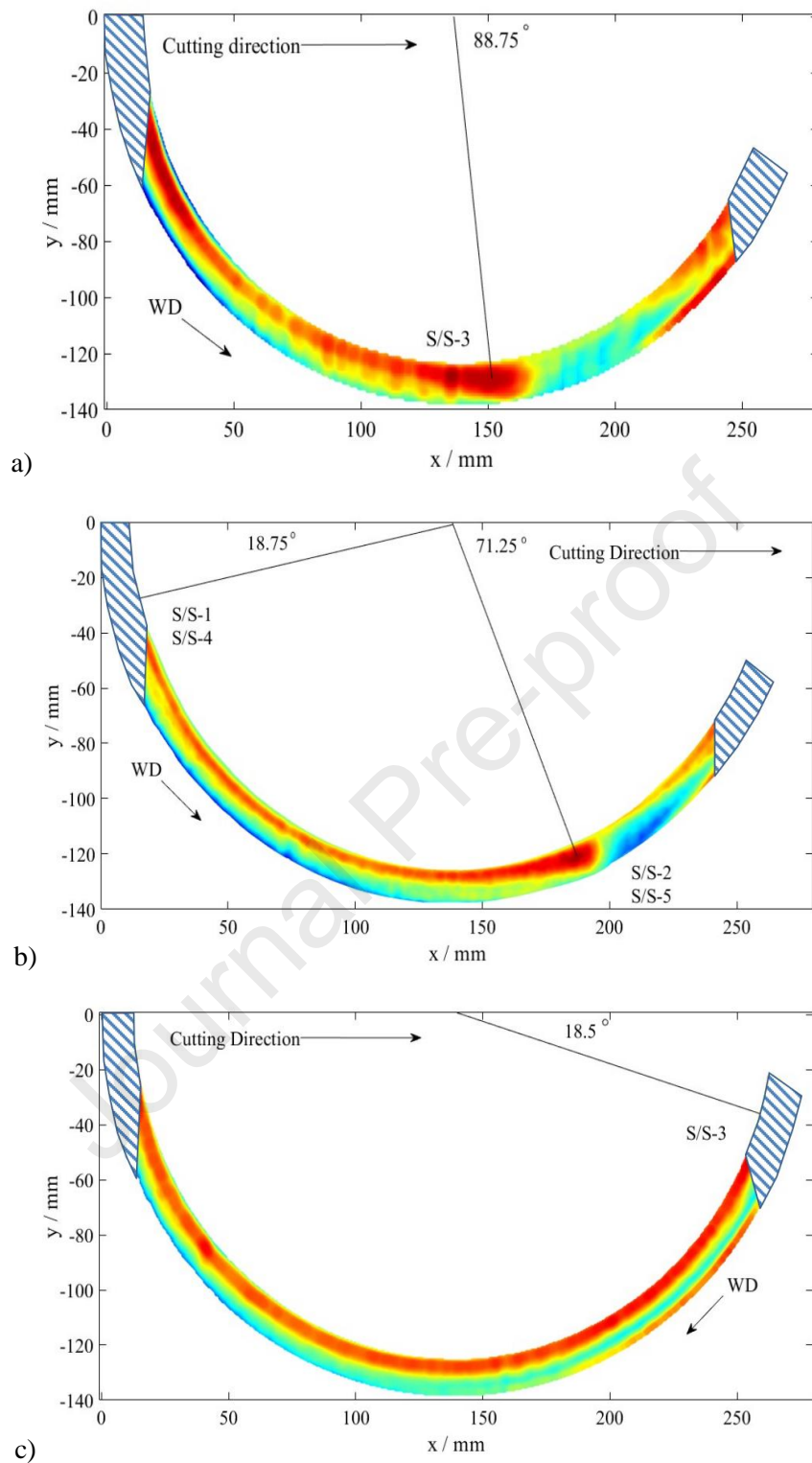
Figure 7 Map of axial stresses in the 180° shells of the mock-ups (a) 3P-HH 180° shell containing weld pass 3 start/stop position at 88.75° clockwise from the axial-radial cut surface, (b) 5P-LH 180° shell containing weld pass 5 start/stop position at 71.25° clockwise from the axial-radial cut surface and c) 5P-LH 180° shell containing weld pass 3 start/stop position at 18.5° clockwise from the axial-radial cut surface.

3.2   Neutron Diffraction

Neutron diffraction residual stress measurments were carried out at the ENGINE-X time of flight neutron diffraction instrument. After the radial-axial contour cuts for hoop stress measurment, one 180° shell of each mock-up pipe was used for neutron diffraction measurement over a radial-axial plane 90° away from the contour cut (see Figure 3). The acquisition of lattice parameter was performed using a 2 x 2 x 2 mm^3 gauge volume on the entire set of measurements on both the welded mock-ups and stress-free reference samples. Following contour method measurements a block of 90 mm x 50 mm x 9 mm was extracted from one of the 180° shells of each mock-up pipe to make stress-free reference samples for neutron diffraction stress-free lattice parameter (d_0) measurements. Two reference pins, 3.5 mm in diameter, were machined from each of the blocks using wire EDM process; a cross-weld 90 mm long pin with the weld centre line at mid-length of the pin and a short 9 mm in length extracted through the wall thickness at the weld centre line. Schematic drawings of the stress-free reference pins and their location and orientation with respect to the extract block are shown in Figure 8. Circumferential slits 1 mm in depth and at 6 mm spacing were machined in the long pin to ensure the extracted sample is stress-free. Stress-free lattice parameter measurements were made at seven points for each of two short pins that go through the wall thickness at weld centre line and eleven measurement points for each of the long pins that ran across the weld in the transverse normal plane.
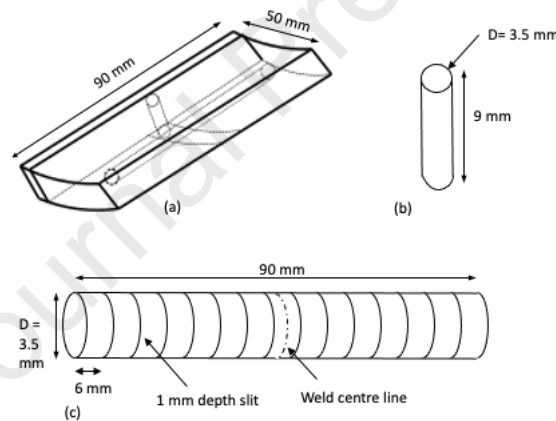

Figure 8 Schematic drawing of (a) an extracted block from $180°$ shell of each mock-up pipe following a contour cut to make stress-free reference samples for neutron diffraction measurements, (b) a short through thickness stress-free reference pin extracted from the block at the weld centre line, (c) a cross-weld longitudinal stress-free reference pin extracted from the block.

The neutron diffraction experiment was simulated using SSCANSS [36] for accurate positioning of the pipe and measurement points. The strain in three orthogonal directions was measured on 38 locations. Each measurement point in the parent material was exposed for 30 minutes and an additional 10 minutes of exposure time was applied to the points in the weld region. The neutron differation measurements were made within $\pm$30 mm of the weld centre line (WCL). The measurement points on the weld centre line and Heat Affected Zone (HAZ) are 1.6 mm away from the inner and outer surfaces of the pipe and there is a 1.5 mm vertical distance between centres of the gauges such that the guage volumes have approximately 50% overlap. There is a 6mm distance between each measurement point on each horizontal path. Overall, a set of 38 neutron diffraction residual stress

measurement points was made on each pipe. Figure 9 shows the hoop stress measured using neutron diffraction together with the location of the measurement points on each weld cross section.
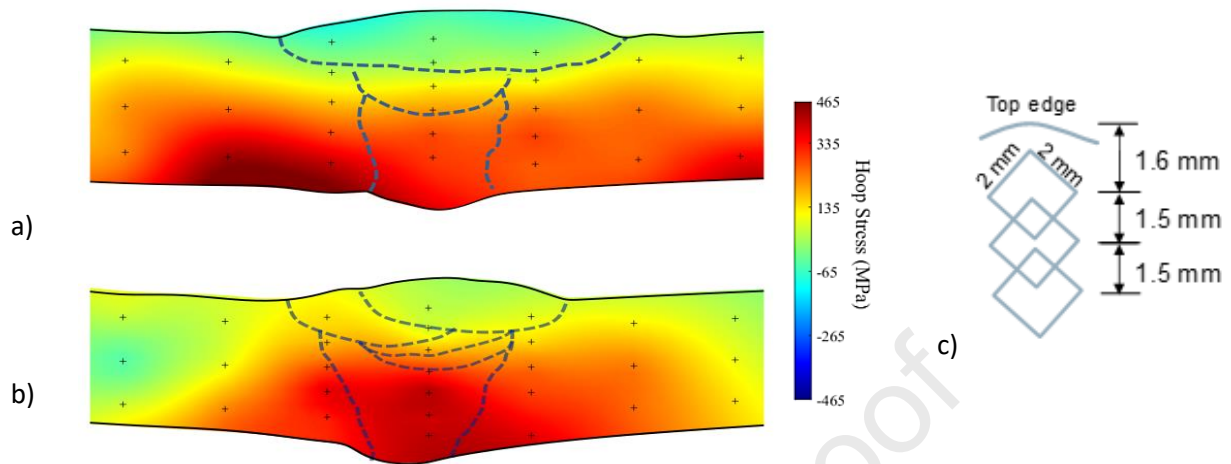

Figure 9 Maps of hoop stress over an axial-radial plane of the weld region measured by neutron diffraction for (a) 3P-HH, (b) H5P-LH mock-ups; superimposed with the measurement locations as modelled in SSCANSS software and (c) a depiction of the gauge volume size also showing the typical distance from top edge that was kept at all times and a depiction of the measurement locations in the through thickness direction.

To compare the contour results with neutron diffraction stresses on a fair basis, the contour hoop stresses were averaged over neutron diffraction gauge area, 2 mm x 2 mm. The contour and neutron diffraction line profiles are compared in Figure 10 and Figure 11 for 3PHH and 5P-LH mock-ups respectively. Note that contour stresses averaged over ND gauge area show the stress values at the ND measurement points while the smooth line profiles show the Gaussian point average stress values (75% averaging, ABAQUS output) along the defined paths.
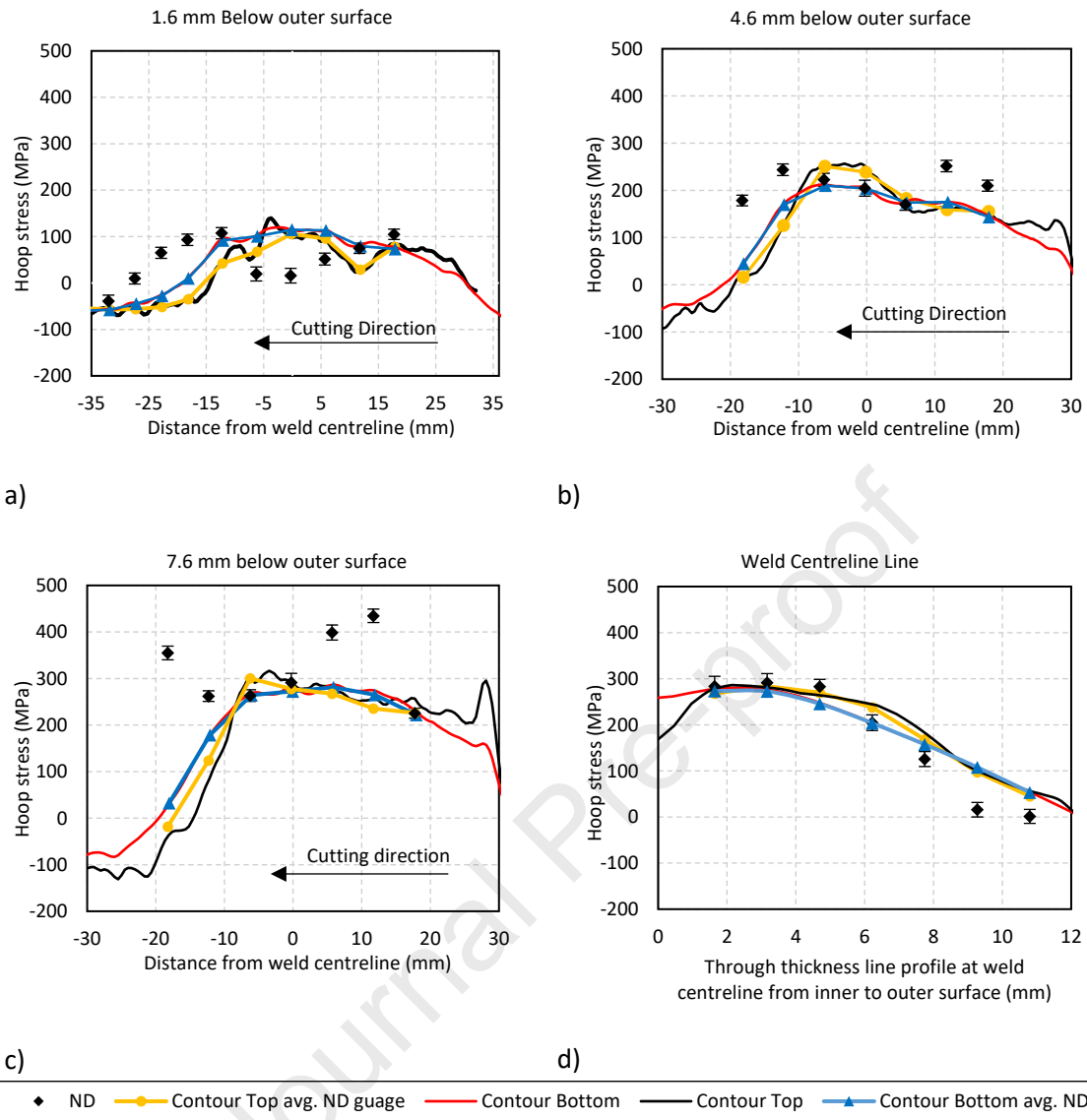
Figure 10 Comparison of contour and neutron diffraction measurements for 3P-HH mock-up along a line profile at a) 1.6 mm, b) 4.6 mm, c)7.6 mm below the outer surface and d) weld centreline.
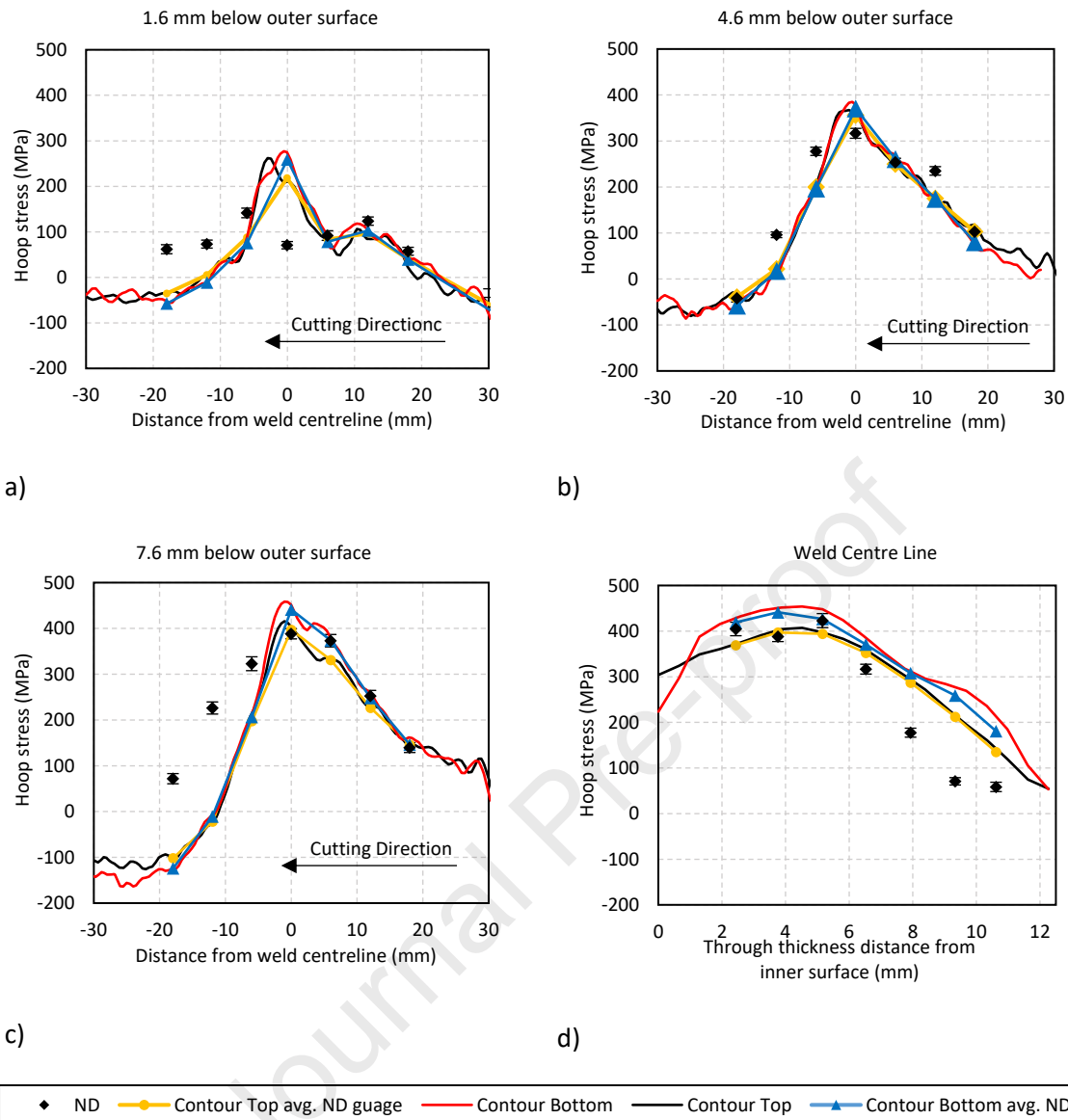
Figure 11 Comparison of contour and neutron diffraction measurements for 5P-LH mock-up along a line profile at a) 1.6 mm b) 4.6 mm c) 7.6 mm below the outer surface and d) weld centreline.

Figure 12 presents the distribution of axial stress along three line profiles across the weld centre line for both mock-ups.
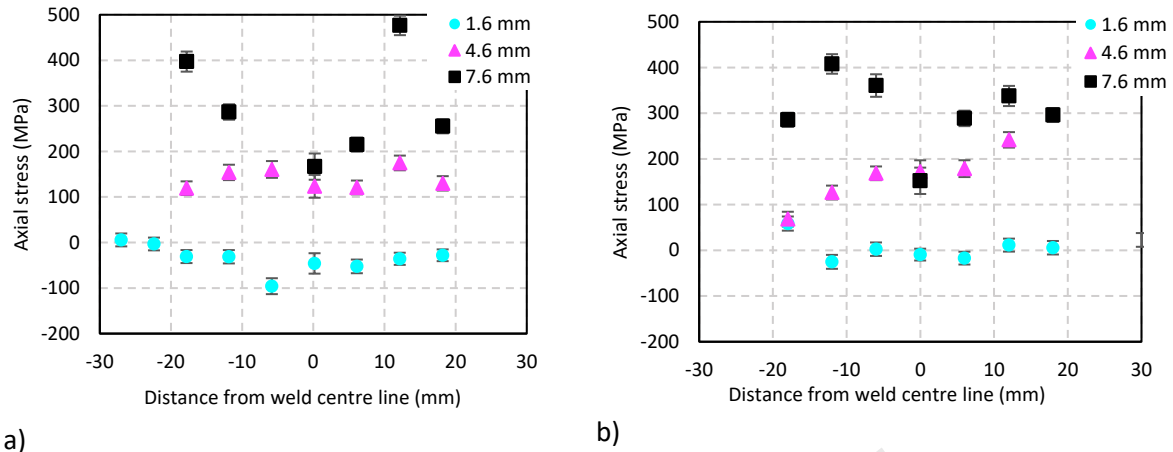
a)

b)

Figure 12 Neutron diffraction Axial stress distribution along line profiles at 1.6 mm, 4.6 mm and 7.6 mm below the outer surface for (a) 3P-HH mock-up and (b) 5P-LH mock-up.

4   Discussion of results

The axial-radial contour cut planes were specifically chosen in the steady state welding region away from weld start/stop positions for two reasons; (a) to allow neutron diffraction measurements to be made at similar welding condition for direct comparison with contour measurements and (b) to allow radial-hoop contour cut plane to be made on the remaining 180° shells for characterising the signature of weld start/stop position on the axial stress distribution.

The single cut approach bisecting two wall thicknesses simultaneously led to capturing the distribution of hoop bending stress and its variation along the length of the pipe together with self-equilibrated hoop residual stress. The 2D map of hoop stress presented in Figure 5 for both mock-ups show symmetry features on the distribution of hoop stress on both wall thicknesses. This symmetry feature is also evident in line profile distribution of hoop stress for Top and Bottom wall thicknesses presented in Figure 10 and Figure 11 for the 3P-HH and 5P-LH mock up respectively. This is as expected due to the contour cut plane being made at steady state weld region. For both mock-ups the through-wall distribution of hoop stress in the weld region present the maximum tensile stress at the weld root, near the inner surface of the pipe, with decreasing magnitude towards the weld cap near the outer surface of the pipe. The extent of tensile stress region in the 3P-HH pipe is over a larger area compared to the 5P-LH pipe. For each pipe the hoop stress map in the vicinity of the weld region for the Top surface is overlaid onto the respective weld macrograph and is presented in Figure 13.

The contour method hoop stress measurement on the 3P-HH mock-up (see Figure 13a) shows the maximum tensile region is off-cantered with respect to the weld centre line and is extended beyond the fusion zone of the weld root pass towards the contour cut direction. For the 5P-LH whilst the maximum tensile stress is measured at the weld centre line some asymmetric features are observed in the tensile stress region with respect to the weld centre line. Similar features are evident in neutron diffraction hoop stress maps (Figure 9). The maximum tensile stress in the 3P-HH mock up is in the order of 300 MPa compared to 450 MPa for the 5P-LH mock up. These welds are manufactured from AISI 316L steel, which cyclically hardens strongly and rapidly [11, 20]. The HAZ and the first few passes in the five-pass weld will have suffered a higher number of thermo-mechanical cycles than in the three-pass weld, thus will have accumulated a longer plastic path, and work hardened to a higher yield strength. The higher stresses are thus exactly what we would expect.
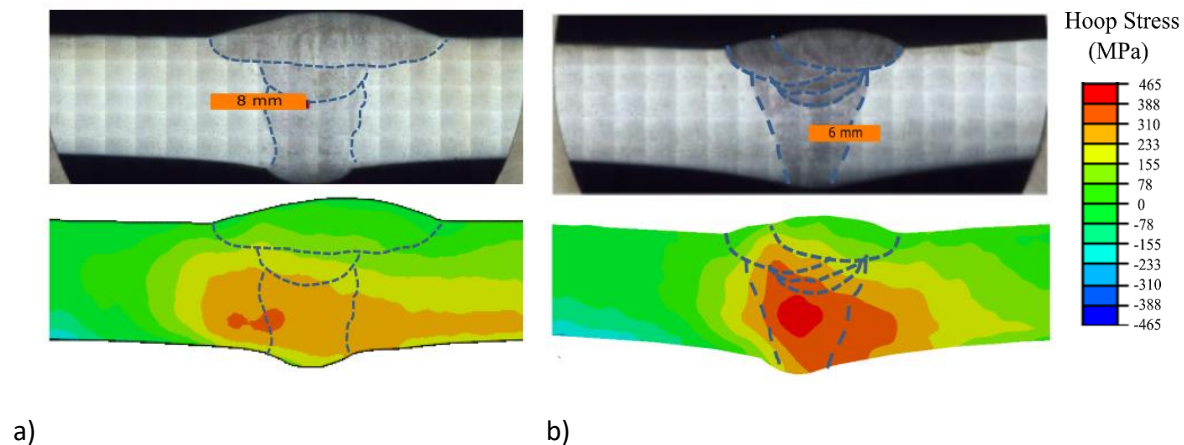
a)   b)

Figure 13 Weld macrograph and contour hoop stresses of the Top surface overlaid on the macrograph for (a) 3P-HH and (b) 5P-LH mock-ups.

The detailed comparison of the contour and neutron diffraction measurements presented in Figure 10 and Figure 11 for 3P-HH and 5P-LH mock-ups respectively shows there is overall a good agreement between the hoop stress results made using the two techniques. There is, however, some discrepancies observed between the neutron diffraction and contour method measurements; for example, the line profile at 7.6 mm below the outer surface of the 3P-HH pipe, see Figure 10c. The neutron diffraction hoop stresses reach 400 MPa whereas the contour hoop stresses are about 280 MPa across ±20 mm of the weld centreline. The three-pass weld is expected to show symmetric behaviour. The skewed feature of the tensile region along the contour cutting direction observed in the map of contour hoop stress and the maximum tensile stresses lower than ND measurements is suspected to be evidence of cutting-induced plasticity error in the contour method measurement for 3P-HH pipe despite the implementation of self-constraint cutting strategy. The 5P-LH pipe has an offset final capping pass. It is therefore excepted to show some asymmetry features in at least the measured hoop stresses. However the asymmetry feature in the map of hoop stresses measured using the contour method is in the opposite direction to that expected from the bead layup (See Figure 13b). Similar asymmetric features, although to lesser extent, are also observed in the map of hoop stress measured using neutron diffraction (see Figure 9a). The ND measurements are likely to exhibit scatter, and interpretation of "positional uncertainty" in these highly deformed pipes is difficult. If anything, we judge that the ND measurements are more symmetric than the contour measurements, not less.

The measured out of plane displacements of the radial-hoop contour cuts on all three 180° shells presented strong evidence of cutting induced artefacts at the start and end of the cut despite the use of sacrificial materials to create a uniform cut plane cross-section. The wire EDM cutting artefact induced region contains the location of weld pass 1 and 4 start/stop position for 5P-LH pipe measuring 161.25 degrees clockwise as shown in Figure 7b and the location of weld pass 3 start/stop position for 5P-LH pipe at 18.5 degree measuring clockwise as shown in Figure 7c.   The stress results for these regions should be discarded and are not presented in Figure 7. For the 5P-LH and 3P-HH 180° shells containing the last weld pass (see Figure 7a & b) the location of the weld stop position is immediately apparent with a high tensile stress region in the wake of the weld stop position followed by the compressive region. The welding direction is marked on the plots. The magnitude of tensile axial stress steadily increases along the welding direction moving towards the weld stop position for both 3P-LH and 5P-HH pipes, reaching the maximum of 262 MPa and 253 MPa respectively.

Figure 7c presents the distribution of axial stress for 5P-LH 180° shells in the weld steady state region noting that the measured axial stress at the location of weld pass 3 start/stop position was discarded due to wire induced cutting artefacts. The axial stress is relatively uniformly distributed with high in magnitude tensile stress region near the inner surface and low level of compressive stresses near the outer surface of the pipe. This observation of axial stress distribution in the steady state weld region show similar trends to neutron diffraction measurements presented in Figure 12.

The axial stress distribution along several angular positions for the three 180° shells are presented in Figure 14. In consistent with the axial stress maps the through-wall line profiles at the location of last weld pass show greater tensile axial stress in magnitude, see Figure 14a and b. It is evident that the trends of axial stress distribution for the two 180° shells containing the last weld pass start/stop position are not consistent at different angular positions on the radial-hoop plane. For the 5P-LH 180° shell containing steady state welding region, Figure 14c, the axial stress line profiles at different angular positions show a relatively more consistent trend and magnitude as presented in Figure 14c. The axial stress levels are lower in magnitude, ranging from maximum of 200 MPa in tension near the inner surface to minimum value of about -230 MPa in compression close to the outer surface.

The neutron diffraction through-wall axial stresses measured at weld centre line in the weld steady state region are also added to the results in Figure 14 for comparison. As expected the neutron diffraction axial stresses show a better agreement with contour axial stresses for the 5P-LH 180° shell containing steady state welding region albeit with slightly higher tensile stresses half way towards the inner surface (see Figure 14c).

a)
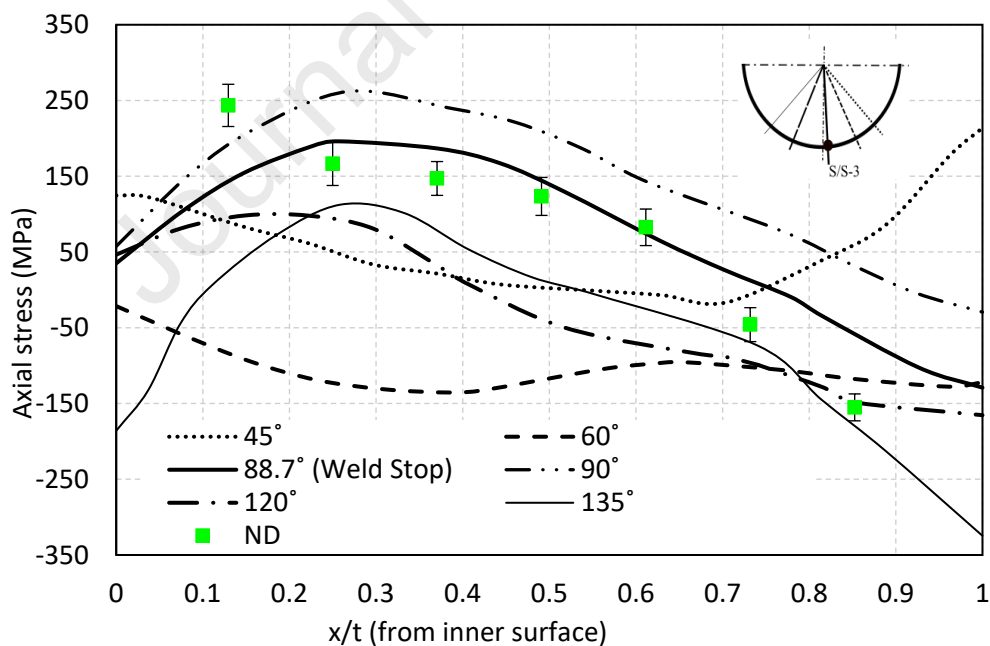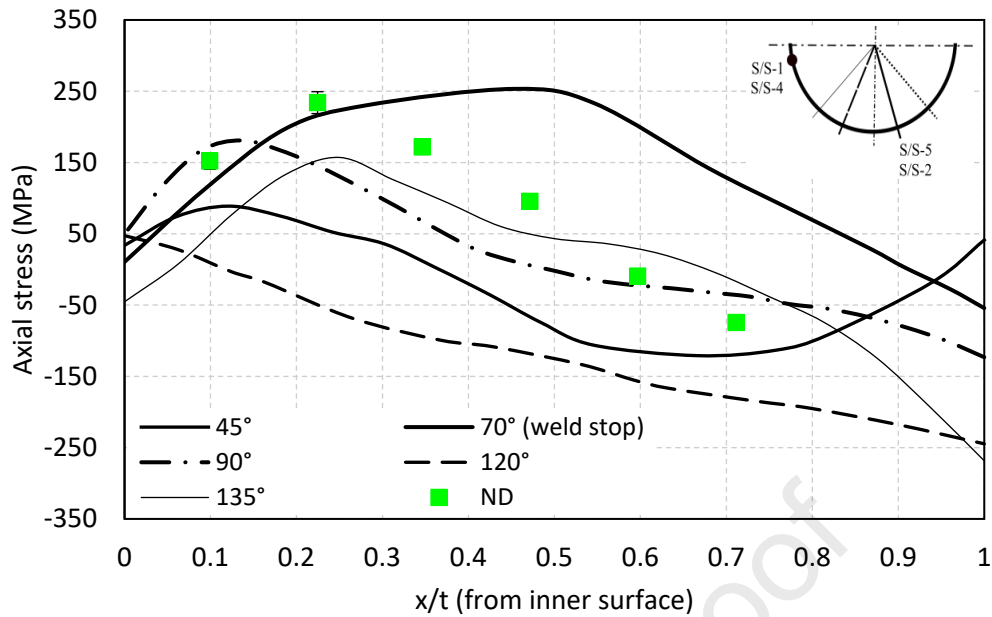
b)
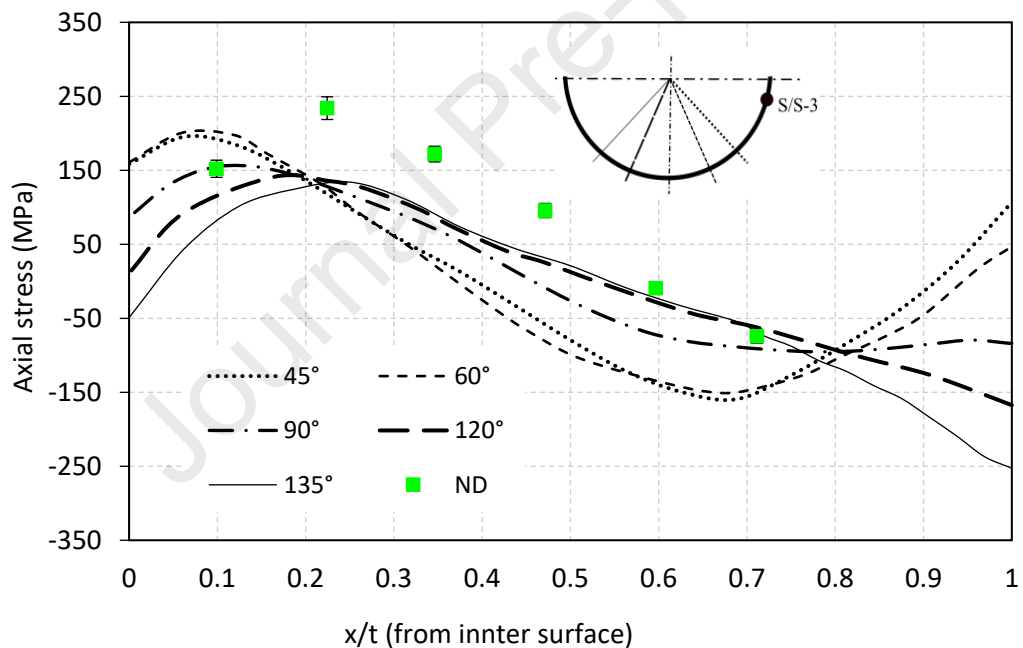
c)

Figure 14 Through thickness line profiles of axial stress measured by the contour method at different angular positions for (a) 3P-HH on the shell with weld pass 3 start/stop position b) 5P-LH on the shell with weld pass 2 and 5 start/stop and weld pass 1 and 4 start/stop positions, and (c) 5P-LH on the shell with weld pass 3 start/stop position. The distance from inner to the outer surface of the pipes are normalised with respect to their thickness. The neutron diffraction through-wall axial stresses measured at weld centre line are also added for comparison.

It is notable that the measured through thickness axial stress distribution in both thin-walled mock-ups (5P-LH and 3P-HH) is not similar to thicker pipes where the region near the inner surface is shown to have lower stress than the outer surface [3].

5   Conclusion

Weld residual stress in two girth-welded thin-walled austenitic mock-up pipes was measured in the hoop and axial directions using the contour method and the results were verified by measurements made using neutron diffraction.

The contour method on the mock-ups were made using a single cut strategy to map the hoop stress distribution on both wall thicknesses simultaneously. The contour method hoop stress distribution for both samples showed symmetry features on both wall thicknesses indicating a uniform stress distribution along the circumference in the weld steady region.

Both techniques measured higher maximum tensile hoop stress in the 5P-LH mock-up compared to the 3P-HH sample. The distribution of hoop stress measured by both techniques showed symmetric features about the weld centre line for the 5P-LH mock-up whereas the maximum tensile region for the 3P-HH sample was observed outside the fusion zone of the weld root pass.

The hoop-radial contour cuts revealed the axial stress distribution signatures of the welding process. The weld stop positions were featured with maximum tensile region in the wake of the weld stop position followed by the compressive region. Through-wall distribution of axial stress line profiles showed variations at different angular positions for the 180° shells containing weld stop positions. In the absence of weld stop position for the 180° containing steady state weld region the measured axial stresses were tensile close to the inner surface and compressive near the outer surface.

The findings in this work are in agreement with the expected effects of thickness and R/t on residual stress profiles, previously described by Bouchard [3]. The behaviour may be summarised as follows:

- In thin-walled pipes with relatively few passes, such as those in the current study the residual stress distribution is dominated by through-wall bending, driven by tourniquet contraction of the entire weld line.
- As the thickness increases, along with the number of weld passes, a cosinusoidal distribution of stress is superposed on any through-wall bending, driven by the deformations induced around individual passes. An example of this is the 35mm wall thickness weld measured and modelled in [37, 38].

6   Acknowledgements:

7   References

1.   *R6 Revision 4, Assessment of the Integrity of Structures Containing defects, Amendment 3, BEGL procedure*. 2004: EDF Energy, Gloucester, UK.

2.   Rissaki, D.K., et al., *Residual stress prediction of arc welded austenitic pipes with artificial neural network ensemble using experimental data.* International Journal of Pressure Vessels and Piping, 2023. **204**: p. 104954.

3.   Bouchard, P.J., *Validated Residual Stress Profiles for Fracture Assessments of Stainless Steel Pipe Girth Welds.* International Journal of Pressure Vessels and Piping, 2007. **84**: p. 195-222.

4.   Mathew, J., et al., *Prediction of residual stresses in girth welded pipes using an artificial neural network approach.* International Journal of Pressure Vessels and Piping, 2017. **150**: p. 89-95.

5.   Mathew, J., et al., *Through-Thickness Residual Stress Profiles in Austenitic Stainless Steel Welds: A Combined Experimental and Prediction Study.* Metallurgical and Materials Transactions A, 2017. **48**(12): p. 6178-6191.

6.   *BS7910:2013, Guide to methods for assessing the acceptability of flaws in metallic structures, British Standards Institution*. 2013.

7.   *Fitness for Service, API 579-1/ASME FFS-1, Second Edition*. 2007.

8.   Smith, M.C. and A.C. Smith, *Advances in weld residual stress prediction: A review of the NeT TG4 simulation round robin part 1, thermal analyses.* International Journal of Pressure Vessels and Piping, 2018. **164**: p. 109-129.

9.   Smith, M.C. and A.C. Smith, *Advances in weld residual stress prediction: A review of the NeT TG4 simulation round robins part 2, mechanical analyses.* International Journal of Pressure Vessels and Piping, 2018. **164**: p. 130-165.

10.   Yaghi, A., et al., *Residual stress simulation in thin and thick-walled stainless steel pipe welds including pipe diameter effects.* International Journal of Pressure Vessels and Piping, 2006. **83**(11): p. 864-874.

11.   Rathod, D.W., et al., *Residual stresses in arc and electron-beam welds in 130 mm thick SA508 steel: Part 1 - Manufacture.* International Journal of Pressure Vessels and Piping, 2019. **172**: p. 313-328.

12.   Vasileiou, A.N., et al., *Residual stresses in arc and electron-beam welds in 130 mm thick SA508 steel: Part 2 –measurements.* International Journal of Pressure Vessels and Piping, 2019. **172**: p. 379-390.

13.   Kokawa, H., et al., *Arrest of weld-decay in 304 austenitic stainless steel by twin-induced grain boundary engineering.* Acta Materialia, 2007. **55**(16): p. 5401-5407.

14.   Smith, M.C. *Weld Residual Stress Activities Within the ATLAS+ Project*. in *ASME 2018 Pressure Vessels and Piping Conference*. 2018.

15.   Smith, M.C., et al. *Modelling and Measuring Residual Stresses in Pipe Girth Welds: Lessons From the Style Framework 7 Project*. in *ASME 2014 Pressure Vessels and Piping Conference*. 2014.

16.   Smith, D.J., P.J. Bouchard, and D. George, *Measurement and Prediction of Residual Stresses in Thick-section Steel Welds.* Journal of Strain Analysis, 2000. **35**(4): p. 287-305.

17.   Smith, M.C., A.C. Smith, and T. Nicak, *Final Report of the STYLE project, European Commission Seventh Framework Programme Report*. 2014.

18. Vasileiou, A.N., et al., *Development of microstructure and residual stress in electron beam welds in low alloy pressure vessel steels.* Materials & Design, 2021. **209**: p. 109924.

19. Balakrishnan, J., et al., *Residual stress distributions in arc, laser and electron-beam welds in 30 mm thick SA508 steel: A cross-process comparison.* International Journal of Pressure Vessels and Piping, 2018. **162**: p. 59-70.

20. Smith, M.C., et al., *Optimised modelling of AISI 316L(N) material behaviour in the NeT TG4 international weld simulation and measurement benchmark.* International Journal of Pressure Vessels and Piping, 2018. **164**: p. 93-108.

21. Prime, M.B., *Cross-Sectional Mapping of Residual Stresses by Measuring the Surface Contour After a Cut.* Journal of Engineering Materials and Technology, 2001. **123**(2): p. 162-168.

22. Prime, M.B. and A. DeWald, *The Contour Method. In Practical Residual Stress Measurement Methods*, in *Practical Residual Stress Measurement Methods*, G.S. Schajer, Editor. 2013. p. 109-138.

23. Pagliaro, P., et al., *Measuring Multiple Residual-Stress Components using the Contour Method and Multiple Cuts.* Experimental Mechanics, 2010. **50**: p. 187-194.

24. Pagliaro, P., et al., *Meausring Inaccessible Residual Streses using Multiple Methods and Superposition.* Experimental Mechanics, 2010. **51**(7): p. 1123-1134.

25. Prime, M.B. and A.L. Kastengren. *The Contour Method Cutting Assumption: Error Minimization and Correction*. in *SEM Annual Conference*. 2010. Indianapolis, Indiana.

26. Hosseinzadeh, F., P. Ledgard, and P.J. Bouchard, *Controlling the Cut in Contour Residual Stress Measurements of Electron Beam Welded Ti-6Al-4V Alloy Plates.* Experimental Mechanics, 2013. **53**(5): p. 829-839.

27. Hosseinzadeh, F., J. Kowal, and P.J. Bouchard, *Towards Good Practice Guidelines for the Contour Method of Residual Stress Measurement.* The Journal of Engineering, 2014.

28. Achouri, A., et al., *The incremental contour method using asymmetric stiffness cuts.* Materials & Design, 2021. **197**: p. 109268.

29. Muránsky, O., et al., *Investigating optimal cutting configurations for the contour method of weld residual stress measurement.* International Journal of Pressure Vessels and Piping, 2018. **164**: p. 55-67.

30. Muránsky, O., et al., *Evaluation of a self-equilibrium cutting strategy for the contour method of residual stress measurement.* International Journal of Pressure Vessels and Piping, 2018. **164**: p. 22-31.

31. Hosseinzadeh, F., et al., *Mitigating cutting-induced plasticity in the contour method, part 1: Experimental.* International Journal of Solids and Structures, 2016. **94-95**: p. 247-253.

32. Muránsky, O., et al., *Mitigating cutting-induced plasticity in the contour method. Part 2: Numerical analysis.* International Journal of Solids and Structures, 2016. **94-95**: p. 254-262.

33. Kim, H.K., et al., *Mitigating Cutting-Induced Plasticity Errors in the Determination of Residual Stress at Cold Expanded Holes Using the Contour Method.* Experimental Mechanics, 2022. **62**(1): p. 3-18.

34. Hosseinzadeh, F. and P.J. Bouchard, *Mapping Multiple Components of the Residual Stress Tensor in a Large P91 Steel Pipe Girth Weld Using a Single Contour Cut.* Experimental Mechanics, 2013. **53**(2): p. 171-181.

35.   Corp, D.S.S., *ABAQUS/Standard User's Manual, Version 6.14.* 2014.

36.   James, J.A., et al. *Use of a Virtual Laboratory to plan, execute and analyse Neutron Strain Scanning experiments*. in *Proc. NOBUGS, NIST*. 2002. Gaithsburg.

37.   Smith, M.C., et al., *Validated prediction of weld residual stresses in austenitic steel pipe girth welds before and after thermal ageing, part 1: Mock-up manufacture, residual stress measurements, and materials characterisation.* International Journal of Pressure Vessels and Piping, 2019. **172**: p. 233-250.

38.   Xiong, Q., et al., *Validated prediction of weld residual stresses in austenitic steel pipe girth welds before and after thermal ageing, part 2: Modelling and validation.* International Journal of Pressure Vessels and Piping, 2019. **172**: p. 430-448.

Highlights:

- "A single cut" contour method approach on thin-walled welded pipes to map the hoop stress distribution on two wall thicknesses simultaneously.

- The multiple-cut contour method to determine 2D map of axial stress distribution in thin walled welded mock ups

- First-of-a kind full field mapping of individual stress components in thin-walled welded pipes for which measured residual stress data in the open literature is sparse.

- Verification of multiple-cut contour method approach using neutron diffraction measurements.

- Insight of weld residual stress signitures in thin walled pipes in the weld steady region and at the location of weld stop positions.

Author statement:

Foroogh Hosseinzadeh: Conceptualisation, Methodology, Writing-Review & Editing, Visualisation and Supervision.

Behrooz Tafazzoli-Moghaddam: Software, validation, Formal analysis, Investigation, Writing-Original draft.

Ho Kyeom Kim: Investigation, Formal analysis.

Peter John Bouchard: Conceptualisation, Methodology, Supervision.

Vasileios Akrivos: Investigation, Formal analysis.

Anastasia N. Vasileiou: Methodology, Writing-Review & Editing.

Mike Smith: Conceptualisation, Methodology, Writing-Review & Editing.

Declaration of interests

☒ The authors declare that they have no known competing financial interests or personal relationships that could have appeared to influence the work reported in this paper.

☐ The authors declare the following financial interests/personal relationships which may be considered as potential competing interests: